ASME Journal of Biomechanical Engineering
Online journal at:
https://asmedigitalcollection.asme.org/biomechanical

Evaluation of an Inverse Method for Quantifying Spatially Variable Mechanics

Daniel P. Pearce[1]
Department of Biomedical Engineering,
University of Wisconsin-Madison,
1550 Engineering Drive, ECB 2139,
Madison, WI 53706
e-mail: dppearce@wisc.edu

Colleen M. Witzenburg[1]
Mem. ASME
Department of Biomedical Engineering,
University of Wisconsin-Madison,
1550 Engineering Drive, ECB 2139,
Madison, WI 53706
e-mail: witzenburg@wisc.edu

Soft biological tissues often function as highly deformable membranes in vivo and exhibit impressive mechanical behavior effectively characterized by planar biaxial testing. The Generalized Anisotropic Inverse Mechanics (GAIM) method links full-field deformations and boundary forces from mechanical testing to quantify material properties of soft, anisotropic, heterogeneous tissues. In this study, we introduced an orthotropic constraint to GAIM to improve the quality and physical significance of its mechanical characterizations. We evaluated the updated GAIM method using simulated and experimental biaxial testing datasets obtained from soft tissue analogs (PDMS and TissueMend) with well-defined mechanical properties. GAIM produced stiffnesses (first Kelvin moduli, K1) that agreed well with previously published Young's moduli of PDMS samples. It also matched the stiffness moduli determined via uniaxial testing for TissueMend, a collagen-rich patch intended for tendon repair. We then conducted the first biaxial testing of TissueMend and confirmed that the sample was mechanically anisotropic via a relative anisotropy metric produced by GAIM. Next, we demonstrated the benefits of full-field laser micrometry in distinguishing between spatial variations in thickness and stiffness. Finally, we conducted an analysis to verify that results were independent of partitioning scheme. The success of the newly implemented constraints on GAIM suggests notable potential for applying this tool to soft tissues, particularly following the onset of pathologies that induce mechanical and structural heterogeneities. [DOI: 10.1115/1.4066434]

Keywords: biaxial testing, anisotropic material behavior, spatial heterogeneity, inverse methods, laser micrometry, experimental validation

Introduction

Soft biological tissues, like heart valves [1,2], myocardium [3–5], skin [6–9], and the sclera [10–12], rely on complex, fibrous extracellular matrices for structure and support during large in vivo deformations. Many of these tissues are thin [13–15], making planar biaxial testing an attractive and relevant loading modality for characterizing their passive mechanical behavior [7,12,16–20]. Traditionally, planar biaxial testing, which was developed for characterization of polymers in the mid-20th century, relies on assumptions of negligible shear forces at the sample boundary and a homogeneous deformation in the sample center [21–23]. These assumptions are reasonable for mechanically isotropic and homogeneous soft materials, but are often inappropriate for soft tissues exhibiting mechanical anisotropy and heterogeneity [24].

A variety of inverse approaches have been developed to determine the spatially varying properties of soft tissues. Kroon and Holzapfel [25] developed an inverse method to identify the elastic properties of mechanically anisotropic and heterogeneous samples, and applied it to saccular cerebral aneurysms subjected to inflation testing. Their method successfully identified parameters governing stiffness, nonlinearity, and collagen fiber orientation and produced wall stress estimates useful for assessing aneurysm rupture risk [25]. Genovese et al. [26] applied another inverse approach [27,28] to inflation testing data obtained from gallbladders. While they determined different regions of the gallbladder exhibited drastically different stiffnesses, the gallbladder was largely isotropic across its surface [26]. Davis et al. [29] inflated ascending thoracic aortic aneurysms and applied their inverse method to quantify the heterogeneous distributions in elastic properties. Accounting for heterogeneous mechanical properties resulted in more accurate predictions of the sample's stress–strain response.

Advances in digital image correlation (DIC) [30–32] and boundary force acquisition [24] have helped overcome classic limitations of planar biaxial testing, offering researchers access to unprecedented information regarding the full-field mechanical behavior of soft tissues. Our Generalized Anisotropic Inverse Mechanics (GAIM) method leverages two-dimensional DIC and state-of-the-art load cells to quantify the spatially variable properties of mechanically anisotropic, heterogeneous soft tissues undergoing planar biaxial extensions [4,33–35]. Our testing protocol was intentionally designed to induce asymmetric, heterogeneous strain states in each sample, enabling GAIM to identify and distinguish regions of geometrical and mechanical heterogeneity [4,24,33]. Initially, GAIM was applied to simulated data from linearly elastic, mechanically anisotropic, and heterogeneous materials and assumed both linear strain and a linearly elastic relationship between stress and strain [33]. Shortly after, GAIM was updated

[1]Corresponding authors.

Manuscript received February 20, 2024; final manuscript received August 14, 2024; published online September 30, 2024. Assoc. Editor: Malisa Sarntinoranont.

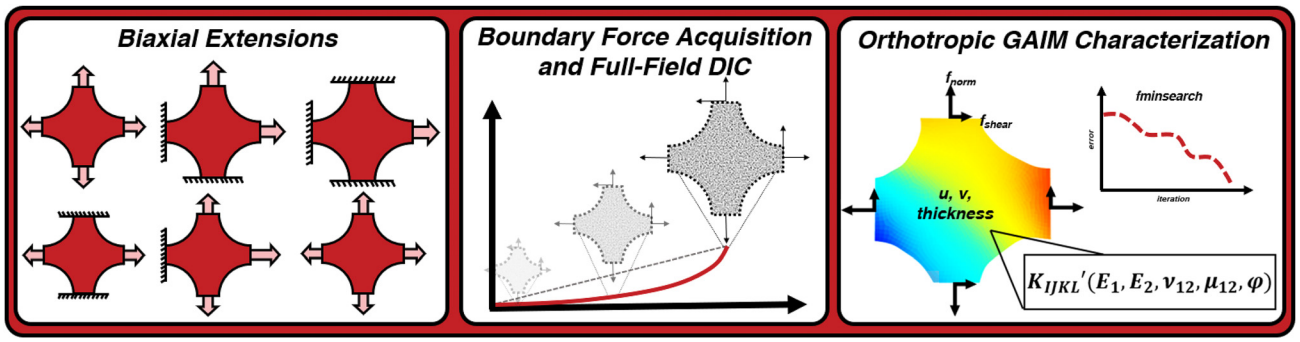

Fig. 1 The updated GAIM method relies on rich planar biaxial testing data, including normal and shear boundary forces during fifteen unique biaxial extensions measured by a combination of 1DOF and 6DOF load cells, full-field displacements from DIC, and full-field thickness contours from laser micrometry. This data is input into GAIM to iteratively solve for constants of the St. Venant orthotropic stiffness tensor using an optimization routine implemented in MATLAB.

to account for large, nonlinear deformations and was applied to rodent right ventricle. These results indicated that decellularization had a negligible effect on the tissue's passive mechanical properties [4]. Recently, GAIM identified substantial mechanical heterogeneity in cerebral aneurysms, which corresponded to regions of highly variable collagenous architecture depicted via second harmonic generation imaging [35]. Despite these successful applications of GAIM [4,34,35], a troubling limitation has been its tendency to produce nonpositive definite stiffness tensors and strain energy functions. In an ongoing effort to improve GAIM for soft tissue mechanics and to maximize the utility of the rich datasets produced during our biaxial testing protocol [24], we introduced a generally orthotropic constraint to GAIM (Fig. 1). In this study, we evaluate the orthotropic GAIM method on a variety of simulated and experimental samples with well-documented mechanical properties [36–38]. We also compare our generally orthotropic solutions to simpler, more computationally affordable mechanically isotropic solutions to further highlight the necessity of accounting for mechanical anisotropy, heterogeneity, and sample geometry during soft tissue characterizations. Finally, we pair GAIM with full-field laser micrometry to distinguish between spatial differences in thickness and stiffness.

Methods

Soft Tissue Analogs. To test our updated GAIM method for mechanically characterizing soft tissues, we opted to use polydimethylsiloxane (PDMS) gels and TissueMend (TEI Biosciences and Stryker Corporation), a Class II FDA-approved patch for soft tissue repair. Both materials have been well-studied and mechanically characterized in literature and offer reliable baseline properties for comparison [36–38]. PDMS generally exhibits linear elasticity following preconditioning, mechanical isotropy, and homogeneity in both its mechanical behavior and structure. TissueMend, a surgical patch designed to emulate the in vivo mechanical function of tendons, exhibits nonlinear force–displacement relationships, pseudoelasticity upon preconditioning, mechanical homogeneity, and mechanical anisotropy, effectively mimicking tendons and making it a useful soft tissue analog for evaluating our updated method [24,37,38]. Additionally, TissueMend is a commercially available product, that, until now, has only been characterized uniaxially [38].

To assess GAIM's ability to characterize materials exhibiting mechanical isotropy and homogeneity, we cast thin PDMS (*thin* PDMS; 10:1 base-to-curing agent ratio) gels of nominally uniform thickness (1 mm). To assess its ability to capture mechanical isotropy and heterogeneity, we cast PDMS gels of varying thickness (1–5 mm, left to right; *thick* PDMS; 10:1 base-to-curing agent ratio). To demonstrate its ability to quantify both stiffness and mechanical anisotropy in a fibrous soft material, we selected TissueMend (*standard* TissueMend). Our workflow for these protocols, which were applied computationally and experimentally, is depicted in Fig. 1 and detailed in Pearce et al. [24]. To examine GAIM's ability to quantify mechanical anisotropy and heterogeneity within the same sample, we also regionally exposed a TissueMend sample to collagenase (*collagenase-treated* TissueMend). The left side of this sample was exposed to collagenase (1 mg/mL; Advanced Biomatrix 5030-50MG) for 1.5 h to degrade and weaken its collagenous matrix, then removed and rinsed in chilled PBS (0.01 M) to limit continued degradation.

Generalized Anisotropic Inverse Mechanics Analysis. The GAIM method assumes a linear anisotropic relationship between Green strain and the second Piola-Kirchoff stress tensor at static equilibrium (St. Venant's model), taking the form:

$$S_{\mathrm{IJ}} = K_{\mathrm{IJKL}} E_{\mathrm{KL}} \tag{1}$$

where S_{IJ} is the second Piola-Kirchoff stress tensor, K_{IJKL} is a fourth-order generalization of the linear elasticity tensor, referred to as the St. Venant stiffness tensor, and E_{KL} is the Green strain tensor [4]. The associated stress balance is:

$$\left(F_{\mathrm{mI}} K_{\mathrm{IJKL}} E_{\mathrm{KL}}\right)_{,J} = 0 \tag{2}$$

where F is the deformation gradient tensor. Using the Galerkin finite element method [33], this relationship can be discretized and simplified to:

$$M = A\mathcal{K} \tag{3}$$

where M is a vector of measured nodal forces, $\mathcal{K}$ is a vector of K_{IJKL} terms for all elements, and A is a matrix consisting of displacements and the remaining terms leftover after discretization [33]. As seen in Eqs. (1)–(3), GAIM is nonlinear in terms of kinematics, but linear in kinetics. This simplification reduces computational cost and promotes a well-posed inverse problem, but neglects the strain-stiffening behavior of many soft tissues.

It is necessary to partition each sample into groups of elements to create an overdetermined system of linear equations [33,39]. Using the original form of GAIM, the overdetermined system can then be solved directly via the least squares method [4,33]. For a biaxial sample under plane stress conditions, this produces six unique stiffness constants for each partition, which describe spatial variations in mechanics across the sample's surface. Allowing the stiffness tensor for a single partition to take on any form enables mechanical characterization without a priori assumptions regarding mechanical anisotropy; however, this method regularly produces nonpositive definite stiffness tensors lacking physical relevance. Constraining GAIM to assume general orthotropy maintains the flexibility necessary to capture the mechanical anisotropy of soft

tissues while ensuring positive-definite stiffness tensors and monotonically increasing strain-energy functions.

Generally Orthotropic Constraint. For a generally orthotropic material, components of K_{IJKL}, the fourth-order St. Venant stiffness tensor (Eq. (1)), are calculated from four unique elastic constants (E_1, E_2, μ_{12}, and ν_{12}) and an angle of rotation (ϕ) between the material's orthogonal axes and the orthogonal axes of the coordinate system [40–42], as seen in Eq. (4) (when $\phi = 0$ deg)

$$K_{IJKL} = \begin{bmatrix} \frac{E_1}{1-\nu_{12}\nu_{21}} & \frac{\nu_{12}E_2}{1-\nu_{12}\nu_{21}} & 0 \\ \frac{\nu_{21}E_1}{1-\nu_{12}\nu_{21}} & \frac{E_2}{1-\nu_{12}\nu_{21}} & 0 \\ 0 & 0 & \mu_{12} \end{bmatrix} \tag{4}$$

E_1 and E_2 are stiffness moduli (corresponding to two orthogonal directional vectors) and must be positive to ensure a positive-definite stiffness tensor; μ_{12} is the shear modulus, which must also be positive; and ν_{12} is a Poisson's ratio [43]. Please note that these elastic constants were assigned the same symbols as they would have in the general Hookean fourth-order stiffness tensor, but are not the same constants since they map finite Green–Lagrange strains to the second Piola-Kirchoff stress tensor here (Eq. (1)). Unlike isotropic linearly elastic materials that conveniently have a Poisson's ratio between $-1 < \nu < 0.5$, ν_{12} can exist outside of these bounds and can be difficult to estimate for generally orthotropic materials. This motivated Li and Barbič [42] to adopt the following approach for estimating ν_{12}, given as:

$$\nu_{12} = \bar{\nu}\sqrt{\frac{E_1}{E_2}} \tag{5}$$

where $\bar{\nu}$, the Poisson's ratio-like parameter used to guide the calculation of ν_{12}, was set to 0.5. When $E_1 = E_2$, this results in $\nu_{12} = 0.5$ and mechanical isotropy. When $E_1 \neq E_2$, ν_{12} will vary based on the ratio between the two directional stiffness moduli. We implemented these constraints [42] on the current GAIM method using an iterative *fminsearch* optimization routine in MATLAB (Mathworks; Natick, MA). In this routine, we initially assumed a single partition, initialized $\mathcal{K}$ such that the material was mechanically isotropic with a stiffness consistent with PDMS, and solved Eq. (3) iteratively. For all experimental and simulated samples presented, this produced a single positive definite fourth-order St. Venant stiffness tensor for each partition. Next, we separated each sample into many smaller partitions and initialized each partition parameter set at the single-partition solution. We then iteratively optimized Eq. (3) for the much longer multipartition form of $\mathcal{K}$. While the iterative modification to GAIM substantially increases computational cost and does not guarantee a unique solution, it enforces production of physiologically relevant positive-definite St. Venant stiffness tensors capable of adopting forms indicative of total mechanical isotropy up to and including general orthotropy.

As in our previous studies [4,34], once we have obtained K_{IJKL} for each partition within a sample, we calculate the eigentensors of the partition's St. Venant stiffness tensor (Eq. (1)), which indicate principal states of stress and strain. The largest eigenvalue, referred to as the first Kelvin modulus ($K1$), represents the sample's stiffness in its stiffest direction for that partition [44]. Its corresponding eigenvector can be used to calculate a strain eigentensor, which defines the partition's preferred stiffness direction. Finally, the two eigenvalues of the strain eigentensor (λ_1 and λ_2) estimate the level of relative mechanical anisotropy (R) in the partition:

$$R = \frac{|\lambda_1 - \lambda_2|}{|\lambda_1 + \lambda_2|} \tag{6}$$

where $R = 0$ for an isotropic sample and $R \rightarrow 1$ for an increasingly mechanically anisotropic sample. Our updated approach produces full-field results, enabling us to quantify the spatial heterogeneity of these variables and to effectively describe a sample's full-field mechanical behavior. In the case of mechanical orthotropy, homogeneity, and linear strains, $K1 = 16.5$ MPa and $R = 0.63$ for an orthotropic sample (like TissueMend) with the following elastic constants: $E_1 = 12$ MPa, $E_2 = 2$ MPa, $\mu_{12} = 1.64$ MPa, and $\nu_{12} = 1.2$.

Isotropic Constraint. For completeness, a mechanically isotropic constraint was also imposed on GAIM. As with the orthotropic constraint, the constants of K_{IJKL} were determined iteratively using the *fminsearch* routine in MATLAB. For this constraint, we assigned the Poisson's ratio, $\nu = 0.49$, and optimized for only the sample's St. Venant in-plane Young's modulus (E_{2D}), which greatly reduced the computational cost of this approach. This method also produced St. Venant stiffness tensors (K_{IJKL}, Eq. (1)) for each partition in the sample, from which full-field distributions of $K1$ were determined. R was 0 by default when mechanical isotropy was imposed. In the case of mechanical isotropy, homogeneity, and linear strain, $K1$ can be related to the Young's modulus by:

$$K1 = \frac{-E}{(\nu - 1)} \tag{7}$$

For an ideal PDMS sample with a Young's modulus of 1.32 MPa and a Poisson's ratio of 0.49, Eq. (7) returns a first Kelvin modulus of 2.59 MPa.

Finite Element Simulations. To test our updated GAIM method with simulated data, we constructed two-dimensional plane stress finite element models in ANSYS WORKBENCH R2021 (ANSYS Inc.; Canonsburg, PA) for simulations of the *thin* PDMS and *standard* TissueMend samples, as well as a three-dimensional model for simulations of the *thick* PDMS sample. Ideal cruciform geometries (Fig. 2, top row) were imported into ANSYS Workbench and meshed using linear Q4 (2D) or linear Hex8 (3D) elements. Both the *thin* and *thick* PDMS simulated samples were assumed to exhibit linear elasticity, mechanical homogeneity, and mechanical isotropy ($E = 1.32$ MPa, $\nu = 0.49$) [36]. The *standard* TissueMend simulated sample was assumed to exhibit linear elasticity, mechanical homogeneity, and orthotropy with its material axes aligned with coordinate axes in ANSYS. The manufacturer does not report any information about TissueMend's stiffness or anisotropy, just that it

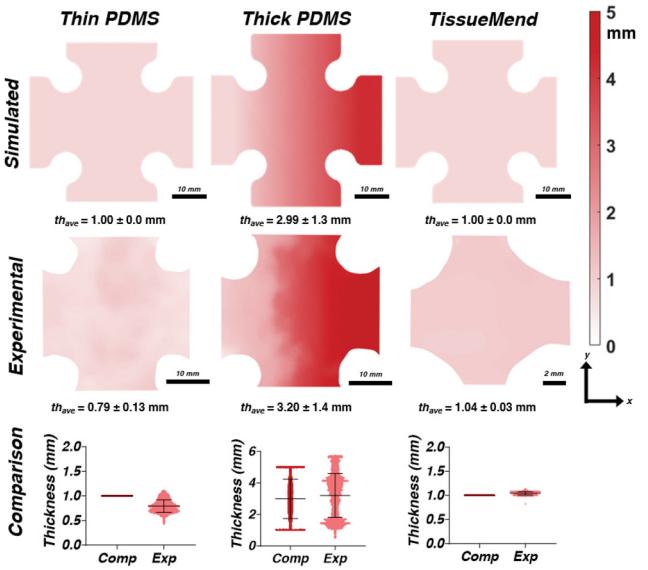

Fig. 2 Simulated and experimental thickness profiles for the *thin* PDMS, *thick* PDMS, and *standard* TissueMend samples. The experimental *thin* sample (nominally cast to be 1 mm thick) was thinner and exhibited more spatial variability in its thickness than expected. Values are presented as mean ± standard deviation.

is derived from fetal bovine dermis. Therefore, using Li and Barbič's approach [42], we set the elastic constants of the *standard* TissueMend sample to $E_1 = 12$ MPa, $E_2 = 2$ MPa, $\mu_{12} = 1.64$ MPa, and $\nu_{12} = 1.2$ based on previously published uniaxial testing results [38] and our preliminary biaxial testing of a single sample [24]. These properties correspond to an orthotropic material approximately six times stiffer along its x-axis compared to its y-axis. H-method refinement was then conducted until average strain values stabilized between successive meshes ($\leq$3%).

In order to replicate the biaxial testing protocols utilized in our experiments [24], we simulated all fifteen unique biaxial extensions (Fig. 1) in ANSYS [24] by applying either fixed constraints (clamps) or displacements to each arm of the sample. Direct solves were used to produce nodal displacements. For the *thick* PDMS simulation, several of the extensions were not solvable directly and were instead resolved using an iterative Newton–Raphson method. The *thin* PDMS and *standard* TissueMend simulations were both subjected to a maximum stretch of 20% (~4.5 mm displacements on each arm) based on their original dimensions, whereas the thick PDMS was subjected to a maximum stretch of 10% (~2.25 mm displacements on each arm). Following completion of each simulation, nodal displacements, normal and shear boundary forces, and the undeformed mesh were exported and used as inputs for the updated GAIM method. All simulations were run serially on a Dell OptiPlex 5090 desktop with an Intel i7-10700 processor, eight cores, 16 logical processors, and 16 GB RAM.

Planar Biaxial Testing. Samples were cast (PDMS) or trimmed (TissueMend) to a standard cruciform shape (Fig. 2, middle row) commonly used in biaxial testing [24,33,45–49]. Each sample was then scanned using a LJ-V7080 class 2 laser micrometer (Keyence; Itasca, IL) to obtain a full-field thickness profile [24]. Both *thin* and *thick* PDMS samples were speckled for DIC using black spray paint, a method we have found to produce fast, affordable, and fine speckle patterns [24,50]. Both *standard* and *collagenase-treated* TissueMend samples were speckled by applying charcoal powder with a fine brush. Following speckling, each sample was secured in our biaxial testing system using a custom gripping system [24]. TissueMend samples were immersed in a saline bath (PBS, 0.01 M) throughout testing. We implemented a combination of one (1DOF; WF12S Miniature Fatigue Resistant Submersible IP65 Load Cells; TestResources Inc., Shakopee, MN) and six degree-of-freedom (6DOF; Nano 17 IP68 F/T Transducers; ATI Industrial Automation, Apex, NC) load cells to capture normal and shear forces at sample boundaries, enabling us to accurately resolve the quasi-static, two-dimensional force balance during mechanical loading. For these experiments, two 1DOF load cells were placed on adjacent actuators and two 6DOF load cells were placed on the remaining two adjacent arms [24]. An overhead camera (Imperx POE-C2400, 2464 × 2056 pixels, 5 Megapixels) and lens (Computar M3Z1228C-MP) were focused on the speckle pattern applied to the sample's surface to enable DIC using robust software developed specifically for soft tissues [30]. Images were obtained at 7 Hz. All images obtained were 2464 × 2056 pixels in size. The following px/mm ratios were calculated: 19.37 px/mm for the *thin* PDMS sample, 25.64 px/mm for the *thick* PDMS sample, 21.18 px/mm for the *standard* TissueMend sample, and 73.29 px/mm for the *collagenase-treated* TissueMend sample.

Prior to testing, each sample was preloaded to a magnitude of $\leq$ 10% of the maximum load reached during testing [51]. Preloads of ~40 kPa, ~20 kPa, and ~0.25 MPa were applied to the *thin* PDMS and *standard* TissueMend samples, the *thick* PDMS sample, and the *collagenase-treated* TissueMend sample, respectively. To achieve a state of pseudo-elasticity, samples were preconditioned with 10 consecutive equibiaxial extensions at a nominal strain level prescribed based on the preloaded grip-to-grip dimensions of each sample (20% for the *thin* and *thick* PDMS and *standard* TissueMend samples and 10% for the *collagenase-treated* TissueMend sample) [4,24,33,51]. Each sample was then subjected to fifteen biaxial extensions (Fig. 1), which were explicitly designed to create asymmetric loading conditions, notable shearing forces, and multiple heterogeneous strain states that better condition GAIM [4,33]. At the end of testing, samples were subjected to one final equibiaxial extension at the desired strain level to ensure pseudo-elasticity was maintained and that minimal damage was inflicted during testing. Raw force signals and images of the sample's surface were exported, processed, and input into GAIM. All mechanical testing was conducted at a strain rate of 1%/s [16,20,24].

Results

Overview of Results. To improve the quality of our soft tissue mechanical characterizations, we introduced an orthotropic constraint to GAIM. We first present laser micrometry results and full-field thickness scans for the *thin* PDMS, *thick* PDMS, and *standard* TissueMend samples and then share each sample's isotropic and orthotropic characterizations from the updated form of GAIM. We then present the orthotropic *collagenase-treated* TissueMend results to further showcase GAIM's ability to detect and quantify mechanical heterogeneity.

Sample Thickness. Figure 2 shows the idealized thickness contours generated for the simulated *thin* PDMS, *thick* PDMS, and *standard* TissueMend samples, as well as the experimental thickness contours obtained using laser micrometry. In general, there was good agreement between simulations and experiments. The *thin* PDMS sample was thinner than anticipated and exhibited higher variability in its thickness. These differences did not preclude mechanical testing and inadvertently show the benefit of including laser micrometry in our protocols, rather than assuming a homogeneous thickness based on traditional methods of thickness measurement [24,26,52]. Simulated and experimental thickness profiles for the *thick* PDMS exhibited similar mean thicknesses (7% difference) and standard deviations (7% difference). Likewise, the mean thickness of the experimental *standard* TissueMend sample showed excellent agreement (4% difference) with its simulated counterpart, both of which displayed small spatial standard deviations.

Isotropic Characterizations. Figure 3 depicts mechanically isotropic characterizations of the two-dimensional behavior of the simulated and experimental samples. Note these characterizations do not include thickness profiles (Fig. 2), resulting in units of N/mm for the in-plane Young's modulus (E_{2D}). The simulated *thin* PDMS sample exhibited an in-plane Young's modulus of 1.17 N/mm from GAIM. When linear strain was input rather than Green strain, GAIM produced an in-plane Young's modulus of $E_{2D} = 1.32$ N/mm, the exact value input into ANSYS (Fig. S1 of the Supplemental Materials on the ASME Digital Collection). GAIM produced a lower in-plane Young's modulus of 0.97 N/mm for the experimental *thin* PDMS sample. The roughly 17% difference between the simulated and experimental in-plane moduli for the *thin* PDMS samples was consistent with the lower mean thickness (0.79 versus 1.0 mm, Fig. 2), likely explaining this discrepancy. GAIM also produced similar mean in-plane Young's moduli for the simulated (3.37 N/mm) and experimental (3.12 N/mm) *thick* PDMS samples, as well as similar variability in the in-plane moduli from left to right. GAIM produced a larger in-plane Young's modulus for the experimental *standard* TissueMend sample (5.83 N/mm) than the simulated sample (2.79 N/mm). We expected this large discrepancy since the simulated sample was modeled as an orthotropic, linearly elastic material in ANSYS and the experimental sample exhibited notable mechanical anisotropy; both samples, however, were treated as mechanically isotropic by GAIM.

Orthotropic Characterizations. Results from the updated orthotropic form of GAIM are shown in Fig. 4. Again, no thickness profiles were included in these results to visualize how the method detects spatial variations in stiffness without full-field thickness

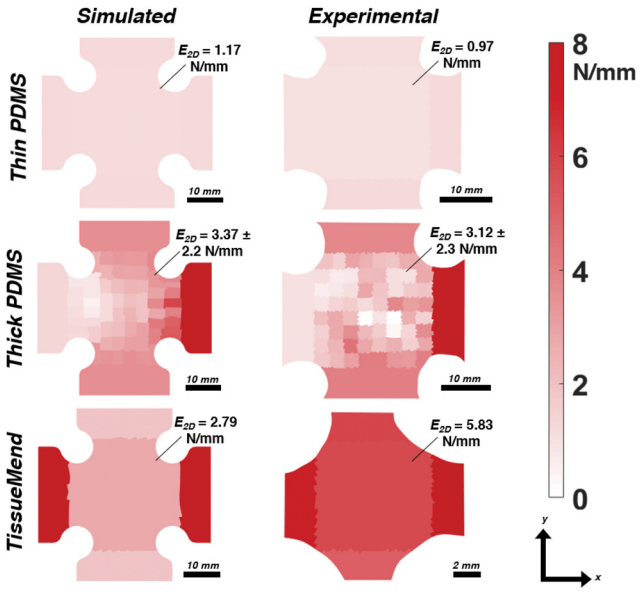

Fig. 3 In-plane Young's moduli (2D; N/mm) for the simulated and experimental *thin* PDMS, *thick* PDMS, and *standard* TissueMend samples when mechanical isotropy was imposed. Call-out values represent the value for the central partition of the sample, unless standard deviations are included, in which case the values represent the mean ± standard deviation of the entire sample.

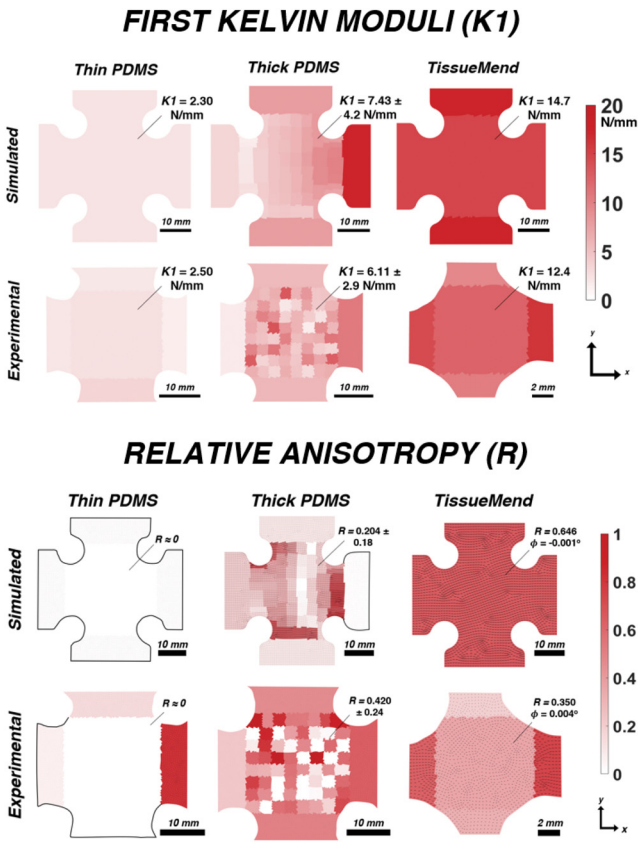

Fig. 4 Mechanical characterizations for the simulated and experimental *thin* PDMS, *thick* PDMS, and *standard* TissueMend samples using the updated orthotropic GAIM method. The first Kelvin Moduli (*K1*, units of N/mm, top) indicates stiffness magnitude and relative anisotropy (*R*, unitless, bottom) indicates the level of mechanical anisotropy. Call-out values represent the value for the central partition of the sample, unless standard deviations are included, in which case the values represent the mean ± standard deviation of the entire sample.

information. For a mechanically isotropic sample with uniform thickness, an in-plane Young's modulus of 1.32 N/mm equates to a first Kelvin modulus of 2.59 N/mm (Eq. (7)). GAIM produced values close to the ideal ($K1 = 2.30$ N/mm; $K1 = 2.50$ N/mm) for the thin simulated and experimental PDMS samples, respectively, with negligible relative anisotropy ($R \approx 0$) in the sample center, indicative of mechanical isotropy. Comparing directional stiffness moduli offers another way of estimating the level of mechanical anisotropy in samples. GAIM produced orthotropic constants $E_1 = E_2 = 1.2$ MPa ($E_1/E_2 = 1$) for the simulated *thin* PDMS sample, again suggesting total mechanical isotropy. For the experimental *thin* PDMS, GAIM produced $E_1 = 1.1$ MPa and $E_2 = 1.4$ MPa ($E_1/E_2 = 0.8$). When linear strain was input rather than Green strain, GAIM produced results perfectly matching ANSYS, $K1 = 2.59$ N/mm, from the simulated data (Fig. S2 of the Supplemental Materials on the ASME Digital Collection). In general, the GAIM results for the experimental *thick* PDMS sample were poor, showing a weak visual trend in stiffness from left to right compared to the steady increase observed in the simulated *thick* PDMS sample. The relative anisotropy metrics produced by GAIM were muddled for both *thick* PDMS samples. As this was the case for both the simulated and experimental *thick* PDMS samples, this result may indicate the limits of GAIM's ability to detect mechanical isotropy in samples with notable three-dimensional structures approaching the limits of standard plane stress analyses [13,15]. GAIM produced a first Kelvin modulus of 14.7 N/mm for the simulated *standard* TissueMend sample ($E_1 = 10.7$ MPa, $E_2 = 1.6$ MPa), which was similar to the first Kelvin modulus of 12.4 N/mm ($E_1 = 8.1$ MPa, $E_2 = 3.7$ MPa) produced for the experimental sample. Mechanical anisotropy results suggested a preference for the long-axis (*x*-axis) in both the simulated and experimental *standard* TissueMend samples. Note the *x*-axis of our biaxial testing machine corresponded to $\varphi \approx 0$ deg for both the experiment and simulation. GAIM estimated less mechanical anisotropy ($R = 0.350$, $E_1/E_2 = 2.2$) in the experimental *standard* TissueMend sample as compared to the simulated sample ($R = 0.646$, $E_1/E_2 = 6.7$). When linear strain was input rather than Green strain, GAIM produced a near perfect result from the simulated TissueMend data, $K1 = 16.5$ N/mm, $R = 0.630$, and $\phi = -0.07$ deg (Fig. S3 of the Supplemental Materials).

Sample Heterogeneity. Figure 5 shows the isotropic characterizations of the simulated and experimental *thick* PDMS samples. GAIM captured an increase in the in-plane Young's modulus of both the samples from their left to right sides (top panel). Once thickness profiles were incorporated into GAIM, we computed the 3D Young's modulus. There were approximately uniform distributions in the Young's modulus from the left to right sides of each sample (ANSYS target: 1.32 MPa) and a trend toward mechanical homogeneity (bottom panel).

Figure 6 includes laser micrometry results, a mechanically orthotropic characterization, and a comparison of 2D and 3D stiffnesses (*K1*) for the *collagenase-treated* TissueMend sample. Laser micrometry indicated thickness varied from ~0.8 to 1 mm from the left (exposed) to right (unexposed) sides of the sample. The 2D mechanically orthotropic characterization captured the collagenase-induced thickness reduction with *K1* increasing steadily from left to right and qualitatively matching the thickness profile. Relative anisotropy was consistent across the sample and appeared unaffected by matrix degradation. Once thickness profiles were incorporated into GAIM, we computed the 3D St. Venant stiffness tensor. The 3D *K1* exhibited a reduced stiffness on the exposed side. This suggests a change in material properties in addition to the reduction in thickness, as spatial differences in *K1* were not fully accounted for by inclusion of the sample's full-field thickness.

Discussion

Planar biaxial testing, popularized in the mid-20th century by polymer scientists, offers a useful testing modality for thin, soft

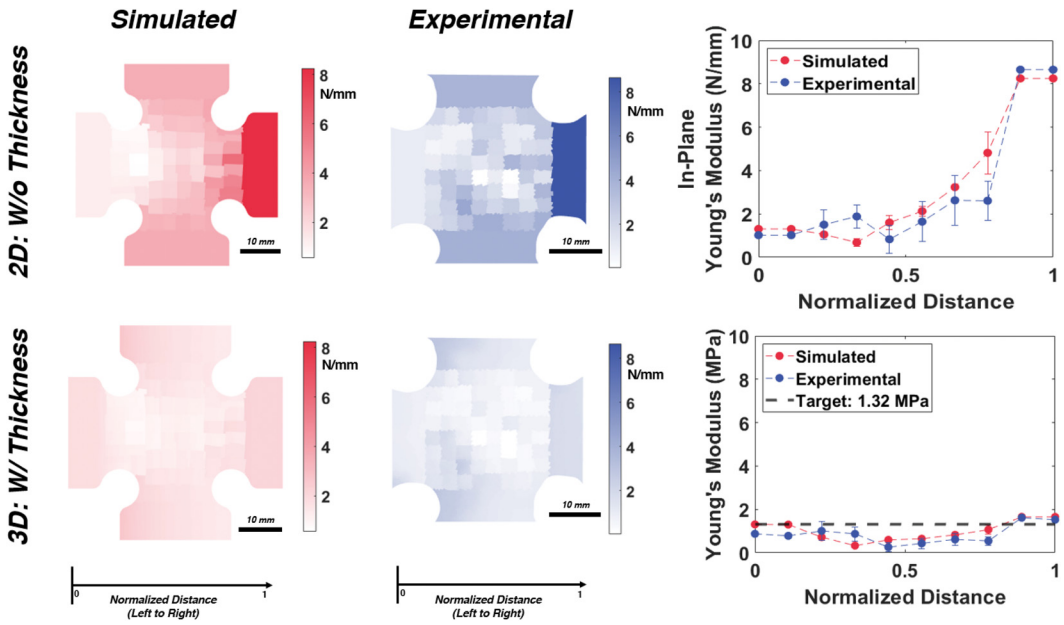

Fig. 5 (Top) The in-plane Young's modulus (2D; N/mm) produced by GAIM for the simulated *thick* PDMS sample (left), the experimental *thick* PDMS sample (center), and from left to right along each sample's vertical centerline (right). (Bottom) The Young's modulus (3D; MPa) produced by GAIM for the simulated *thick* PDMS (left), experimental *thick* PDMS (center), and from left to right along each sample's vertical centerline (right). Target indicates the Young's modulus input into ANSYS.

materials [21–23]. Traditional assumptions of planar biaxial testing – specifically, a homogeneous deformation and the absence of shear forces at the sample's boundary – limit the application of this method to soft biological tissues [24]. Thankfully, advances in DIC and boundary force acquisition have helped overcome these limitations, enabling full-field characterizations of a sample's heterogeneous and anisotropic mechanical properties through various inverse approaches, including our GAIM approach [25,26,29,53,54]. In this study, we introduced a generally orthotropic constraint to GAIM requiring positive-definite stiffness tensors and strain energy functions, thereby improving the physiological relevance of our solutions. We evaluated the updated method using common, well-characterized soft tissue analogs both computationally and experimentally. The constrained GAIM method (Fig. 1), which relies on a series of unique biaxial extensions generating multiple heterogeneous strain states, was used to characterize a PDMS gel of uniform thickness, a PDMS gel of varying thickness, and TissueMend, an FDA-approved surgical patch (Fig. 4). We then paired GAIM with full-field laser micrometry thickness measurements to distinguish between regional differences in stiffness and thickness (Fig. 5). Finally, we characterized a TissueMend sample regionally exposed to collagenase, which we found induced changes in both geometry and material properties (Fig. 6).

Mechanically isotropic characterizations (Figs. 3 and 5) revealed good agreement between simulated and experimental results for PDMS samples. The in-plane Young's modulus for the central partition in the simulated *thin* PDMS sample was 1.17 N/mm, just below the 1.32 N/mm value input into ANSYS. The experimental in-plane Young's modulus was 0.97 N/mm, corresponding to a 17% difference relative to the simulated result. We attribute this discrepancy to the 21% reduction in thickness obtained for the experimental *thin* PDMS sample (Fig. 2), as well as variations in mixing and curing times [36,55]. The excellent agreement between the in-plane Young's modulus (2D) and Young's modulus (3D) for the simulated and experimental *thick* PDMS samples (Fig. 5, right) further implicate thickness as the primary driver of this discrepancy in the *thin* PDMS samples. The *thick* PDMS samples, both simulated and experimental, exhibited an increase in stiffness from left to right (Fig. 5) when analyzed without thickness information. Once the sample's thickness profiles were incorporated, Young's moduli distributions became much more uniform. While all PDMS samples, both simulated and experimental, exhibited linear force–displacement curves during loading, the large deformations imposed during testing caused Green strain to differ substantially from linear strain. This is best demonstrated by the $K1$ produced by GAIM for the *thin* PDMS, which differed by ∼11% depending on the use of linear (Figs. S1 and S2 of the Supplemental Materials on the ASME Digital Collection) or Green (Fig. 3) strain. Note when linear strain was input into GAIM, simulated results aligned exactly with ANSYS, which relied on linear kinematics. As noted by others [56,57], accounting for higher order strain terms when considering PDMS and other similar soft polymers may be crucial for accurately estimating traction forces exerted on substrates by cells [58–60], which are known to undergo large deformations during traction force generation [57,61].

Imposing isotropy decreases computational cost (>50% reduction in runtime, 51 min versus ∼2 h for the *thick* PDMS sample with 36 partitions; ∼90% reduction in runtime for a 68-partition solution, 3.5 h versus 29 h), but totally restricts GAIM's ability to estimate mechanical anisotropy [4,7,16]. For both the simulated and experimental *thin* PDMS samples, GAIM produced a relative anisotropy, R, of zero when general orthotropy was permitted. This was further supported by a comparison of directional stiffness moduli, E_1 and E_2, which were identical ($E_1/E_2 = 1$) for the simulation and comparable for the experiment ($E_1/E_2 = 0.8$). This demonstrated that the constrained GAIM method could correctly identify the sample's level of mechanical alignment (or the lack thereof) without any additional impositions. There was a ∼9% difference between the simulated ($K1 = 2.30$ N/mm) and experimental ($K1 = 2.50$ N/mm) stiffness metrics. As shown in Fig. S2 of the Supplemental Materials, when linear strain was input into GAIM, simulated results aligned exactly with ANSYS. In contrast, relative anisotropy results were poor for the simulated and experimental *thick* PDMS samples. This finding may highlight a limit of GAIM for identifying mechanical anisotropy in samples with geometries approaching the bounds of standard plane stress analyses [13,15]. For the simulated *thick* PDMS sample, the length-to-maximum thickness ratio was 10 (the limit for assuming plane stress [15]), and for the experimental *thick* PDMS sample it was only

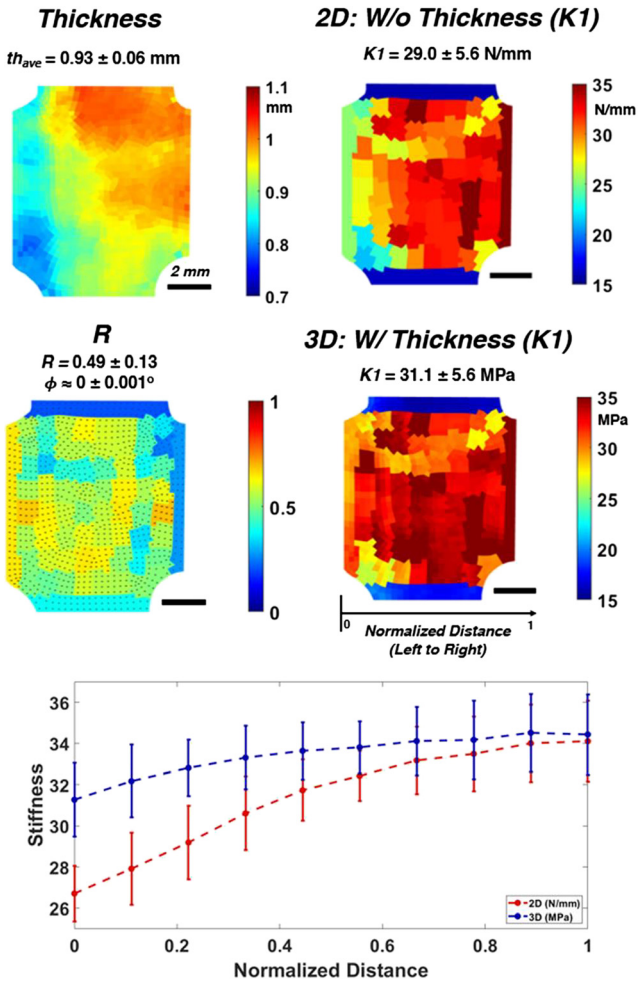

Fig. 6 Thickness profile, first Kelvin modulus (2D; N/mm), relative mechanical anisotropy, and first Kelvin modulus (3D; MPa) distributions for the *collagenase-treated* TissueMend sample. The difference in stiffness between the 2D and 3D results along the sample's vertical centerline (bottom) suggests a change in material properties not fully explained by inclusion of the full-field thickness data. Values presented as mean ± standard deviation of the entire sample.

6.2, suggesting out-of-plane deformations of this sample type likely violate plane stress assumptions. While we were unable to measure out-of-plane deformation, the 6DOF load cells we utilized in the biaxial testing protocol measure out-of-plane forces in addition to normal and shear forces at the sample boundary. For the experimental *thin* PDMS sample, the out-of-plane forces were miniscule (< 1% of the maximum normal force for any extension), but were more considerable for the experimental *thick* PDMS sample (reaching 5% of the maximum normal force in some extensions).

Characterizations of TissueMend samples revealed good agreement between simulated and experimental stiffness magnitudes and directions of mechanical alignment, as well as with stiffnesses reported by others [38]. There was a modest difference between the first Kelvin moduli of the simulated ($K1 = 14.7$ N/mm) and experimental ($K1 = 12.4$ N/mm) *standard* TissueMend samples. In both cases, the large first Kelvin moduli corresponded to the x-axis of our testing system ($\varphi \approx 0°$ for both the simulated and experimental samples) and relative anisotropy indicated moderate (experimental, $R = 0.35$) to strong (simulated, $R = 0.65$) mechanical alignment. To our knowledge, this is the first reported biaxial mechanical characterization of TissueMend. Lacking prior characterizations, we assigned idealized properties in ANSYS based on our preliminary work with TissueMend [24] and linear moduli reported from uniaxial testing [38]. Discrepancies between simulated and experimental results could indicate TissueMend is less anisotropic than our preliminary experiment indicated. They could also be a result of the linear orthotropic model implemented in ANSYS, or the linear kinetic relationship imposed by the GAIM method, as opposed to the nonlinear anisotropic behavior exhibited by the sample during testing. Lastly, Derwin et al. [38] reported high intersample variability in linear moduli (∼15 ± 3.5 MPa) and a natural product like bovine dermis likely causes high intersample variability in anisotropy as well. If off-axis loading is important to its use, we recommend additional mechanical investigations into TissueMend's anisotropic behavior. There were also differences in TissueMend sample shape between the simulations and experiments. Specifically, the experimental TissueMend sample was smaller and had rounded corners with larger radii (relative to its full dimensions) than the simulated sample since it was trimmed to a cruciform shape using a biopsy punch and razor blade [24]. One benefit of our GAIM method in combination with full-field DIC [30] and laser micrometry is that it accounts for small, nonideal sample geometries. This is a particularly valuable feature for application to soft tissues and tissue analogs, for which forming an ideal shape is challenging since samples must be cut rather than cast. Furthermore, our use of full-field DIC [30] and 6DOF load cells allow us to capture any shear strains or shear forces that may arise from sample shape asymmetry.

The orthotropic mechanical characterization of the *collagenase-treated* TissueMend sample produced a mean $K1$ of 29.0 ± 5.6 N/mm, with the unexposed side around 35 N/mm and the exposed side around 25 N/mm prior to inclusion of full-field thickness profiles (Fig. 6). Following incorporation of the thickness profile, the unexposed side remained unperturbed with $K1$ of ∼35 MPa. The exposed side increased slightly to a $K1$ of ∼32 MPa but did not reach 35 MPa, suggesting a subtle reduction in the sample's stiffness in addition to the change in thickness. Local caliper measurements are commonly used to measure a soft tissue's thickness prior to mechanical testing, but only provide one (or a few, if taken in multiple locations) thickness value for the sample [24,26,52]. While convenient, this technique makes it challenging to distinguish between geometrical and mechanical heterogeneity and may result in poor estimations of a sample's true material properties. Full-field thickness measurements enable accurate and reliable descriptions of a soft tissue's mechanical properties and the stresses it is subjected to during loading. Although GAIM may be used to mechanically characterize homogeneous samples, this experiment demonstrates that the method truly excels at describing heterogeneous variations across the surface of a sample (Fig. 6). This ability makes GAIM an attractive method for studying pathologies that disrupt and alter the mechanical and structural properties of soft biological tissues.

Limitations and Future Directions. Other investigators have also sought to quantify mechanical anisotropy and heterogeneity in soft tissues. Similar to GAIM, Kroon and Holzapfel [25] employed an iterative error-minimizing routine to produce orthotropic descriptions of a soft tissue's mechanical behavior. They relied on the classic constitutive model presented by Holzapfel, Gasser, and Ogden (HGO) [62] to characterize idealized saccular cerebral aneurysms geometries during inflation. Genovese et al. [26] implemented a pointwise inverse method to study the anisotropic and nonlinear mechanical behavior of the gallbladder and found it exhibited isotropic mechanical behavior across the majority of its surface when subjected to bulge inflation testing. Using another pointwise approach, Davis et al. [29] applied bulge inflation testing and their inverse method to ascending thoracic aortic aneurysms. They fitted mechanical testing data to a modified HGO model [63] and determined the mechanical properties of their aneurysmal samples to be notably heterogeneous. More recently, Gasparotti et al. [64] relied on their past bulge testing data [65] and a two fiber-family modified HGO [62] to numerically determine that elliptical sample shapes produced higher quality descriptions of anisotropic

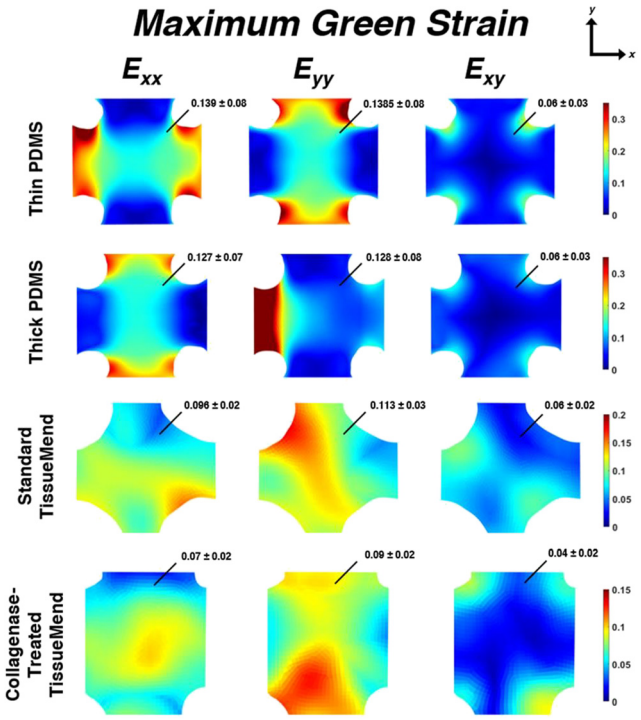

Fig. 7 Maximum Green strain across all fifteen biaxial extensions for each element in each sample. All samples were extended to 20% grip strain, except for the *collagenase-treated* TissueMend sample, which was extended to 10% grip strain. Call-out values indicate spatial mean ± standard deviation.

soft tissues, like those taken from aortic aneurysms. An advantage of our inverse method [24] from previous studies in that it relies on variations of classic planar biaxial testing rather than inflation.

Inflation testing produces deformations similar to equibiaxial testing and both modalities are physiologically relevant for many soft tissues [4,25,26,29,33,35]. However, our protocol [24] supplements traditional equibiaxial testing to induce a number of asymmetric, heterogeneous strain states. Figure 7 shows the maximum Green strain for all fifteen biaxial extensions for each element in each sample for this study. While the spatial maximum normal strain is comparable to a single equibiaxial extension, the shear strain is generally higher, particularly in the sample center (Fig. S6 of the Supplemental Materials on the ASME Digital Collection). This protocol broadens the strain space used to condition GAIM and identify mechanical heterogeneity in samples. Technical advancements this method employs include 6DOF load cells to measure normal and shear boundary forces, fast and affordable DIC to quantify full-field deformations, and laser scanning micrometry to obtain full-field sample thickness [24,26,52]. The combination of laser micrometry and DIC also enable prescription of experimental sample shape, which is of particular importance for soft tissues and tissue analogs, for which forming an ideal shape is challenging since samples must be cut rather than cast. The experimental results included here reiterate the importance of full-field deformation and normal and shear boundary force measurements when mechanically characterizing fibrous samples with variable geometrical and structural (Fig. 6) compositions [24].

A major limitation of our inverse method is that the constitutive equation is nonlinear in terms of kinematics, but assumes linear kinetics (Eq. (1)). The inclusion of nonlinear constitutive relationships (such as the HGO model) by other researchers better capture the nonlinear kinetics commonly exhibited by soft biological tissues [25,26,29,66–68]. While the assumption of linear kinetics greatly reduces the computational cost and complexity of our inverse approach, the effects we observed in this study when nonlinear kinematics were considered suggest it may be important to address. To evaluate this further, we assumed homogeneity and used the St. Venant stiffness tensor constants from the central partition of the *thin* PDMS (Fig. 3) and *standard* TissueMend samples (Fig. 4) and the measured Green–Lagrange strain in the same region to compute a GAIM-derived first Piola-Kirchoff stress. Figure S5 of the Supplemental Materials on the ASME Digital Collection shows stress in the vertical and horizontal directions as a function of the corresponding Green–Lagrange strain. There was a relatively linear relationship between stress and strain for the *thin* PDMS sample, however, there was prominent nonlinearity for the *standard* TissueMend sample. In both cases, the St. Venant model captured the peak stresses experienced by samples at the end of a prescribed deformation well with an error of less than 15%. These results suggest the St. Venant model may be a poor model for describing the transient mechanical behavior of soft tissues, but that the secant modulus is well-suited to estimating peak stress. One way we have proposed to account for nonlinear kinetics in the past was to apply GAIM in a piecewise manner throughout a sample's nonlinear mechanical response to loading [69]. This produces a collection of strain energy or stress values across multiple strain states for each sample element that can then be fitted to a nonlinear constitutive model of the user's choice. The flexibility in constitutive model is a clear benefit of the piecewise approach, which worked well on simulated data sets [69]. When combined with the new constrained version of GAIM presented in this study, which ensures positive-definite St. Venant stiffness tensors and monotonically increasing strain-energy, it has great promise for incorporating nonlinear kinetics into GAIM.

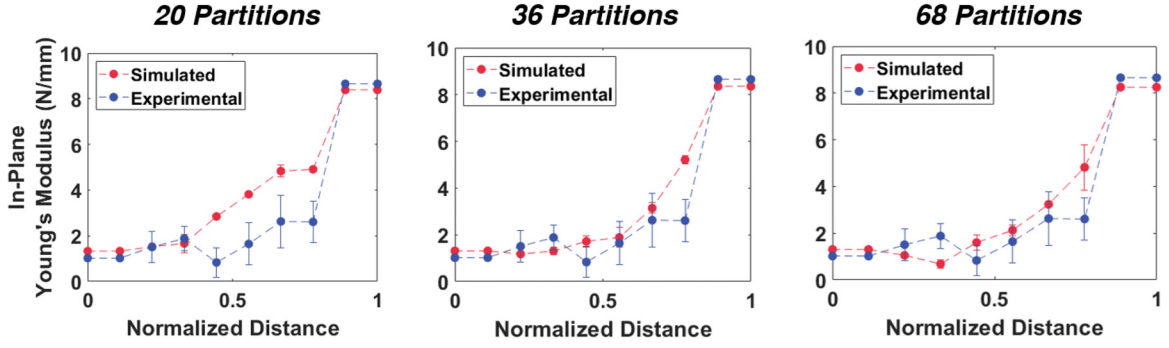

Fig. 8 The in-plane Young's modulus (2D; N/mm) produced by GAIM for the simulated and experimental *thick* PDMS samples (red and blue, respectively) from left to right along the sample's vertical centerline when the number of partitions was increased to 20, 36 and 68

The GAIM method relies on biaxial testing data and assumes plane stress. In general, this assumption is reasonable for samples with a thickness at least one order of magnitude less than their overall length and width [13,15,24], as they do not experience large out-of-plane deformations and forces. While regional stiffness results were good for the simulated (length-thickness ratio: 10.0) and experimental (length-thickness ratio: 6.2) *thick* PDMS samples, relative anisotropy results were poor (Fig. 4). GAIM did not correctly identify either the simulated or the experimental sample as mechanically isotropic. This highlights an important limitation of GAIM and the accompanying biaxial testing protocol for mechanically characterizing samples with pronounced three-dimensional geometries.

Lastly, GAIM is limited in its ability to quantify mechanical heterogeneity by the number, size, shape, and location of partitions. To better understand this limitation, we prescribed increasingly fine partitioning schemes for the experimental and simulated *thick* PDMS samples, such that the number of partitions increased from 20 (Fig. 8) to 36 and 68 (Fig. 5). When we included additional partitions (similar to standard *h*-refinement procedures for finite element analyses), the heterogeneity in stiffness produced for the *thick* PDMS simulated and experimental samples was not altered (Fig. 8). We repeated this process for the *collagenase-treated* TissueMend sample (Fig. S4 of the Supplemental Materials on the ASME Digital Collection). For all partitioning levels, GAIM identified the right side of the sample as stiffer than the left and produced similar values of $K1$ at the sample edges. However, as the number of partitions was decreased, the stiffness distribution no longer monotonically increased from left to right. While overall spatial trends were independent of partitioning, finer spatial comparisons may benefit from partitioning schemes that consider morphology or kinematics [39].

Conclusion

Many soft biological tissues function as highly deformable membranes in vivo, making planar biaxial testing an appealing and physiologically relevant loading modality for characterizations of their mechanical behavior. In this article, we introduced and evaluated a generally orthotropic constraint to our previously demonstrated GAIM method to improve the physical significance and utility of its mechanical characterizations. The orthotropic characterizations of PDMS and TissueMend produced stiffness and mechanical anisotropy metrics consistent with expectations and past studies [36,38,55]. We also demonstrated the benefits of including full-field thickness measurements in GAIM to distinguish between structural and geometrical heterogeneity. The success of the updated orthotropic form of GAIM and our accompanying biaxial protocol in quantifying the experimental mechanical behavior of these highly deformable soft tissue analogs indicates great potential for applying this approach to soft tissues. This is particularly valuable when considering mechanically disruptive pathologies that create unknown spatial variabilities in stiffness, mechanical alignment, and thickness, as well as therapeutic interventions designed to preserve or modulate these properties, tissue function, and patient health.

Acknowledgment

The authors would also like to thank Michael Chiariello, Matt Culver, Cate Eberman, Elizabeth Gunderson, Mark Nemcek, and Shreya Sreedhar for their assistance with projects and lab sessions contributing to this work.

Funding Data

- National Science Foundation Division of Civil, Mechanical, and Manufacturing Innovation (Award No. 2030173; Funder ID: 10.13039/100000147).

Data Availability Statement

The datasets generated and supporting the findings of this article are obtainable from the corresponding author upon reasonable request.

References

[1] Billiar, K. L., and Sacks, M. S., 2000, "Biaxial Mechanical Properties of the Natural and Glutaraldehyde Treated Aortic Valve Cusp—Part I: Experimental Results," ASME J. Biomech. Eng., **122**(1), pp. 23–30.
[2] Ross, C., Laurence, D., Wu, Y., and Lee, C. H., 2019, "Biaxial Mechanical Characterizations of Atrioventricular Heart Valves," J. Vis. Exp., (146), p. e59170.
[3] Sacks, M. S., and Chuong, C. J., 1993, "Biaxial Mechanical Properties of Passive Right Ventricular Free Wall Myocardium," ASME J. Biomech. Eng., **115**(2), pp. 202–205.
[4] Witzenburg, C., Raghupathy, R., Kren, S. M., Taylor, D. A., and Barocas, V. H., 2012, "Mechanical Changes in the Rat Right Ventricle With Decellularization," J. Biomech., **45**(5), pp. 842–849.
[5] Nemavhola, F., 2021, "Study of Biaxial Mechanical Properties of the Passive Pig Heart: Material Characterisation and Categorisation of Regional Differences," Int. J. Mech. Mater. Eng., **16**(1), pp. 1–14.
[6] Lanir, Y., and Fung, Y. C., 1974, "Two-Dimensional Mechanical Properties of Rabbit Skin—I. Experimental System," J. Biomech., **7**(1), pp. 29–34.
[7] Lanir, Y., and Fung, Y. C., 1974, "Two-Dimensional Mechanical Properties of Rabbit Skin—II. Experimental Results," J. Biomech., **7**(2), pp. 171–182.
[8] Schneider, D. C., Davidson, T. M., and Nahum, A. M., 1984, "In Vitro Biaxial Stress-Strain Response of Human Skin," Arch. Otolaryngol., **110**(5), pp. 329–333.
[9] Jiang, M., Sridhar, R. L., Robbins, A. B., Freed, A. D., and Moreno, M. R., 2021, "A Versatile Biaxial Testing Platform for Soft Tissues," J. Mech. Behav. Biomed. Mater., **114**, p. 104144.
[10] Eilaghi, A., Flanagan, J. G., Tertinegg, I., Simmons, C. A., Wayne Brodland, G., and Ross Ethier, C., 2010, "Biaxial Mechanical Testing of Human Sclera," J. Biomech., **43**(9), pp. 1696–1701.
[11] Cruz Perez, B., Tang, J., Morris, H., Palko, J., Pan, X., Hart, R., and Liu, J., 2014, "Biaxial Mechanical Testing of Posterior Sclera Using High-Resolution Ultrasound Speckle Tracking for Strain Measurements," J. Biomech., **47**(5), pp. 1151–1156.
[12] Ndlovu, Z., Desai, D., Pandelani, T., Ngwangwa, H., and Nemavhola, F., 2022, "Biaxial Estimation of Biomechanical Constitutive Parameters of Passive Porcine Sclera Soft Tissue," Appl. Bionics Biomech., **2022**, pp. 1–11.
[13] Humphrey, J. D., 2002, "Cardiovascular Solid Mechanics—Cells, Tissues, and Organs," Springer, New York.
[14] Humphrey, J. D., 1998, "Computer Methods in Membrane Biomechanics," Comput. Methods Biomech. Biomed. Eng., **1**(3), pp. 171–210.
[15] Ventsel, E., and Krauthammer, T., 2001, *Thin Plates and Shells*, CRC Press, Boca Raton, FL.
[16] Demer, L. L., and Yin, F. C., 1983, "Passive Biaxial Mechanical Properties of Isolated Canine Myocardium," J. Physiol., **339**(1), pp. 615–630.
[17] Humphrey, J. D., Strumpf, R. K., and Yin, F. C. P., 1990, "Biaxial Mechanical Behavior of Excised Ventricular Epicardium," Am. J. Physiol., **259**(1), pp. H101–H108.
[18] Vande Geest, J. P., Sacks, M. S., and Vorp, D. A., 2006, "The Effects of Aneurysm on the Biaxial Mechanical Behavior of Human Abdominal Aorta," J. Biomech., **39**(7), pp. 1324–1334.
[19] Nemavhola, F., 2017, "Biaxial Quantification of Passive Porcine Myocardium Elastic Properties by Region," Eng. Solid Mech., **5**(3), pp. 155–166.
[20] Sacks, M. S., 2000, "Biaxial Mechanical Evaluation of Planar Biological Materials," J. Elast. Phys. Sci. Solids, **61**(1), pp. 199–246.
[21] Rivlin, R. S., 1948, "Large Elastic Deformations of Isotropic Materials IV. further Developments of the General Theory," Philos. Trans. R. Soc., A, **241**(835), pp. 379–397.
[22] Rivlin, R. S., and Saunders, D. W., 1951, "Large Elastic Deformations of Isotropic Materials VII. Experiments on the Deformation of Rubber," Philos. Trans. R. Soc., A, **243**(865), pp. 251–288.
[23] Treloar, L. R. G., 1948, "Stresses and Birefringence in Rubber Subjected to General Homogeneous Strain," Proc. Phys. Soc., **60**(2), pp. 135–144.
[24] Pearce, D., Nemcek, M., and Witzenburg, C., 2022, "Combining Unique Planar Biaxial Testing With Full-Field Thickness and Displacement Measurement for Spatial Characterization of Soft Tissues," Curr. Protoc., **2**(7), p. e493.
[25] Kroon, M., and Holzapfel, G. A., 2008, "Estimation of the Distributions of Anisotropic, Elastic Properties and Wall Stresses of Saccular Cerebral Aneurysms by Inverse Analysis," Proc. R. Soc. A, **464**(2092), pp. 807–825.
[26] Genovese, K., Casaletto, L., Humphrey, J. D., and Lu, J., 2014, "Digital Image Correlation-Based Point-Wise Inverse Characterization of Heterogeneous Material Properties of Gallbladder In Vitro," Proc. R. Soc. A, **470**(2167), p. 20140152.
[27] Zhou, X., and Lu, J., 2008, "Inverse Formulation for Geometrically Exact Stress Resultant Shells," Int. J. Numer. Methods Eng., **74**(8), pp. 1278–1302.
[28] Lu, J., Zhou, X., and Raghavan, M. L., 2008, "Inverse Method of Stress Analysis for Cerebral Aneurysms," Biomech. Model. Mechanobiol., **7**(6), pp. 477–486.
[29] Davis, F., Luo, Y., Avril, S., Duprey, A., and Lu, J., 2015, "Pointwise Characterization of the Elastic Properties of Planar Soft Tissues: Application to Ascending Thoracic Aneurysms," Biomech. Model. Mechanobiol., **14**(5), pp. 967–978.
[30] Raghupathy, R., and Barocas, V. H., 2013, "Robust Image Correlation Based Strain Calculator for Tissue Systems (20130022, Dr. Victor Barocas)," accessed

[31] Zhou, B., Ravindran, S., Ferdous, J., Kidane, A., Sutton, M. A., and Shazly, T., 2016, "Using Digital Image Correlation to Characterize Local Strains on Vascular Tissue Specimens," J. Vis. Exp., **2016**(107), p. 53625.
[32] Yang, J., and Bhattacharya, K., 2019, "Augmented Lagrangian Digital Image Correlation," Exp. Mech. **59**(2), pp. 187–205.
[33] Raghupathy, R., and Barocas, V. H., 2010, "Generalized Anisotropic Inverse Mechanics for Soft Tissues," ASME J. Biomech. Eng., **132**(8), p. 081006.
[34] Raghupathy, R., Witzenburg, C., Lake, S. P., Sander, E. A., and Barocas, V. H., 2011, "Identification of Regional Mechanical Anisotropy in Soft Tissue Analogs," ASME J. Biomech. Eng., **133**(9), p. 091011.
[35] Shih, E. D., Provenzano, P. P., Witzenburg, C. M., Barocas, V. H., Grande, A. W., and Alford, P. W., 2022, "Characterizing Tissue Remodeling and Mechanical Heterogeneity in Cerebral Aneurysms," J. Vasc. Res., **59**(1), pp. 34–42.
[36] Johnston, I. D., McCluskey, D. K., Tan, C. K. L., and Tracey, M. C., 2014, "Mechanical Characterization of Bulk Sylgard 184 for Microfluidics and Microengineering," J. Micromech. Microeng., **24**(3), p. 035017.
[37] Aurora, A., McCarron, J., Iannotti, J. P., and Derwin, K., 2007, "Commercially Available Extracellular Matrix Materials for Rotator Cuff Repairs: State of the Art and Future Trends," J. Shoulder Elb. Surg., **16**(5), pp. S171–S178.
[38] Derwin, K. A., Baker, A. R., Spragg, R. K., Leigh, D. R., and Iannotti, J. P., 2006, "Commercial Extracellular Matrix Scaffolds for Rotator Cuff Tendon Repair: Biomechanical, Biochemical, and Cellular Properties," J. Bone Jt. Surg., **88**(12), pp. 2665–2672.
[39] Witzenburg, C., Dhume, R. Y., Lake, S. P., and Barocas, V. H., 2016, "Automatic Segmentation of Mechanically Inhomogeneous Tissues Based on Deformation Gradient Jump," IEEE Trans. Med. Imaging, **35**(1), pp. 29–41.
[40] Jayne, B. A., and Hunt, M. O., 1969, "Plane Stress and Plane Strain in Orthotropic and Anisotropic Media," Wood Fiber Sci., **1**(3), pp. 236–247.
[41] Krenk, S., 1979, "On the Elastic Constants of Plane Orthotropic Elasticity," J. Compos. Mater, **13**(2), pp. 108–116.
[42] Li, Y., and Barbič, J., 2014, "Stable Orthotropic Materials," SCA 2014 - Proceedings of ACM SIGGRAPH/Eurographics Symposium on Compututer Animation, Copenhagen, Denmark, July 21–23, pp. 41–46.
[43] Cowin, S. C., and Mehrabadi, M. M., 1995, "Anisotropic Symmetries of Linear Elasticity," ASME Appl. Mech. Rev, **48**(5), pp. 247–285.
[44] Thomson, W., 1856, "XXI. Elements of a Mathematical Theory of Elasticity," Philos. Trans. R. Soc. London, **146**, pp. 481–498.
[45] Makinde, A., Thibodeau, L., and Neale, K. W., 1992, "Development of an Apparatus for Biaxial Testing Using Cruciform Specimens," Exp. Mech. **32**(2), pp. 138–144.
[46] Boehler, J. P., Demmerle, S., and Koss, S., 1994, "A New Direct Biaxial Testing Machine for Anisotropic Materials," Exp. Mech., **34**(1), pp. 1–9.
[47] Waldman, S. D., and Lee, J. M., 2005, "Effect of Sample Geometry on the Apparent Biaxial Mechanical Behaviour of Planar Connective Tissues," Biomaterials, **26**(35), pp. 7504–7513.
[48] Lecompte, D., Smits, A., Sol, H., Vantomme, J., and Van Hemelrijck, D., 2007, "Mixed Numerical–Experimental Technique for Orthotropic Parameter Identification Using Biaxial Tensile Tests on Cruciform Specimens," Int. J. Solids Struct., **44**(5), pp. 1643–1656.
[49] Jacobs, N. T., Cortes, D. H., Vresilovic, E. J., and Elliott, D. M., 2013, "Biaxial Tension of Fibrous Tissue: Using Finite Element Methods to Address Experimental Challenges Arising From Boundary Conditions and Anisotropy," ASME J. Biomech. Eng., **135**(2), p. 021004.
[50] Estrada, J. B., and Franck, C., 2015, "Intuitive Interface for the Quantitative Evaluation of Speckle Patterns for Use in Digital Image and Volume Correlation Techniques," ASME J. Appl. Mech., **82**(9), p. 095001.
[51] Debes, J., and Fung, Y., 1995, "Biaxial Mechanics of Excised Canine Pulmonary Arteries," Am. J. Physiol., **269**(2), pp. H433–H442.
[52] Lee, J. M., and Langdon, S. E., 1996, "Thickness Measurement of Soft Tissue Biomaterials: A Comparison of Five Methods," J. Biomech., **29**(6), pp. 829–832.
[53] Murdock, K., Martin, C., and Sun, W., 2018, "Characterization of Mechanical Properties of Pericardium Tissue Using Planar Biaxial Tension and Flexural Deformation," J. Mech. Behav. Biomed. Mater., **77**, pp. 148–156.
[54] Avril, S., and Evans, S., 2017, *Material Parameter Identification and Inverse Problems in Soft Tissue Biomechanics*, Vol. 573, Springer International Publishing, Cham.
[55] Ariati, R., Sales, F., Souza, A., Lima, R. A., and Ribeiro, J., 2021, "Polydimethylsiloxane Composites Characterization and Its Applications: A Review," Polymers (Basel), **13**(23), pp. 4258–21.
[56] Long, R., Hall, M. S., Wu, M., and Hui, C. Y., 2011, "Effects of Gel Thickness on Microscopic Indentation Measurements of Gel Modulus," Biophys. J, **101**(3), pp. 643–650.
[57] Toyjanova, J., Bar-Kochba, E., López-Fagundo, C., Reichner, J., Hoffman-Kim, D., and Franck, C., 2014, "High Resolution, Large Deformation 3D Traction Force Microscopy," PLoS One, **9**(4), p. e90976.
[58] Beussman, K. M., Mollica, M., Leonard, A., Miles, J., Hocter, J., Song, Z., Stolla, M., Han, S., Emery, A., Thomas, W., and Sniadecki, N., 2023, "Black Dots: High-Yield Traction Force Microscopy Reveals Structural Factors Contributing to Platelet Forces," Acta Biomater., **163**, pp. 302–311.
[59] Li, H., Matsunaga, D., Matsui, T., Aosaki, H., Kinoshita, G., Inoue, K., Doostmohammadi, A., and Deguchi, S., 2022, "Wrinkle Force Microscopy: A Machine Learning Based Approach to Predict Cell Mechanics From Images," Commun. Biol., **5**(1), pp. 1–3.
[60] Notbohm, J., Napiwocki, B. N., de Lange, W. J., Stempien, A., Saraswathibhatla, A., Craven, R. J., Salick, M. R., Ralphe, J. C., and Crone, W. C., 2019, "Two-Dimensional Culture Systems to Enable Mechanics-Based Assays for Stem Cell-Derived Cardiomyocytes," Exp. Mech., **59**(9), pp. 1235–1248.
[61] Franck, C., Hong, S., Maskarinec, S. A., Tirrell, D. A., and Ravichandran, G., 2007, "Three-Dimensional Full-Field Measurements of Large Deformations in Soft Materials Using Confocal Microscopy and Digital Volume Correlation," Exp. Mech., **47**(3), pp. 427–438.
[62] Holzapfel, G. A., Gasser, T. C., and Ogden, R. W., 2000, "A New Constitutive Framework for Arterial Wall Mechanics and a Comparative Study of Material Models," J. Elasticity, **61**(1–3), pp. 1–48.
[63] Gasser, T. C., Ogden, R. W., and Holzapfel, G. A., 2006, "Hyperelastic Modelling of Arterial Layers With Distributed Collagen Fibre Orientations," J. R. Soc. Interface, **3**(6), pp. 15–35.
[64] Gasparotti, E., Vignali, E., Quartieri, S., Lazzeri, R., and Celi, S., 2023, "Numerical Investigation on Circular and Elliptical Bulge Tests for Inverse Soft Tissue Characterization," Biomech. Model. Mechanobiol., **22**(5), pp. 1697–1707.
[65] Vignali, E., Gasparotti, E., Capellini, K., Fanni, B., Landini, L., Positano, V., and Celi, S., 2021, "Modeling Biomechanical Interaction Between Soft Tissue and Soft Robotic Instruments: Importance of Constitutive Anisotropic Hyperelastic Formulations," Int. J. Rob. Res., **40**(1), pp. 224–235.
[66] Wertheim, M. G., 1847, "Mémoire Sur L'élasticité et la Cohésion Des Principaux Tissus du Corps Humain," Ann. Chim. Phys., **21**, pp. 385–414.
[67] Roy, C. S., 1881, "The Elastic Properties of the Arterial Wall," J. Physiol., **3**(2), pp. 125–159.
[68] Humphrey, J., 2003, "Continuum Biomechanics of Soft Biological Tissues," Proc. Math. Phys. Eng. Sci., **459**(2029), pp. 3–46.
[69] Witzenburg, C., and Barocas, V. H., 2016, "A Nonlinear Anisotropic Inverse Method for Computational Dissection of Inhomogeneous Planar Tissues," Comput. Methods Biomech. Biomed. Eng., **19**(15), pp. 1630–1646.